

Tunable Microelectromechanical Filters that Exploit Parametric Resonance

Jeffrey F. Rhoads and Steven W. Shaw¹
Department of Mechanical Engineering
Michigan State University
2555 Engineering Building
East Lansing, MI 48824
Phone: (517)-432-1085
Fax: (517)-353-1750
Email: rhoadsje@egr.msu.edu, shawsw@egr.msu.edu

Kimberly L. Turner and Rajashree Baskaran²
Department of Mechanical and Environmental Engineering
University of California, Santa Barbara
1171 Engineering Building II
Santa Barbara, CA 93106
Phone: (805)-893-5106
Fax: (805)-893-8651
Email: turner@engineering.ucsb.edu, raji@engineering.ucsb.edu

Abstract

Background: This paper describes an analytical study of a bandpass filter that is based on the dynamic response of electrostatically-driven MEMS oscillators.

Method of Approach: Unlike most mechanical and electrical filters that rely on direct linear resonance for filtering, the MEM filter presented in this work employs parametric resonance.

Results: While the use of parametric resonance improves some filtering characteristics, the introduction of parametric instabilities into the system does present some complications with regard to filtering.

Conclusions: The aforementioned complications can be largely overcome by implementing a pair of MEM oscillators with novel tuning schemes and some processing logic to produce a highly effective bandpass filter.

Key Words: MEMS, Parametric Excitation, Nonlinear Oscillations, Bandpass Filter

1. Introduction

There is a growing demand for effective and efficient signal filters, due to their presence in a wide variety of wireless communications devices, including cellular phones. Most previous work on such filters has focused on conventional electrical filters [1] and their mechanical counterparts [2]. More recently, the introduction of microelectromechanical (MEM) devices into mainstream engineering has opened a promising new path of study regarding the development of filters [3-7]. This promise is founded upon the distinct advantages MEM filters hold over more conventional designs. Specifically, MEM filters are inherently smaller, consume less power to operate, and

¹ Visiting Professor, Department of Mechanical and Environmental Engineering, University of California, Santa Barbara

² Currently employed at Intel Corp., Phoenix, AZ

have the potential to operate with significantly higher quality (Q) factors (in the case of bandpass filters, resonant frequency to bandwidth ratios) [8]. In addition, MEM filters are easy to integrate with electrical circuitry (sometimes on a single chip), are highly tunable, and, most importantly for this work, MEM oscillators can be designed to exhibit parametric resonance [9]. Virtually all MEM bandpass filters proposed to date have utilized features of direct linear resonance to achieve the desired filtering [5-7]. In contrast, here we describe a means of using parametric resonance in MEMS as the basis for filtering.

The paper is arranged as follows. In Section 2 we review some basics regarding filter performance, and in Section 3 some of the general features of parametric resonance and their relevance to filtering are briefly described. In Section 4 the behavior of a parametrically-excited MEM oscillator is analyzed, and in Section 5 we describe a means of manipulating the oscillator's instability zone in a manner that is beneficial for filter design. The required nonlinear tuning of the oscillators is outlined in Section 6, and the logic for creating a bandpass filter using a pair of MEM oscillators is described in Section 7. The paper closes in Section 8 with a brief discussion of the results and some outstanding issues related to this line of work.

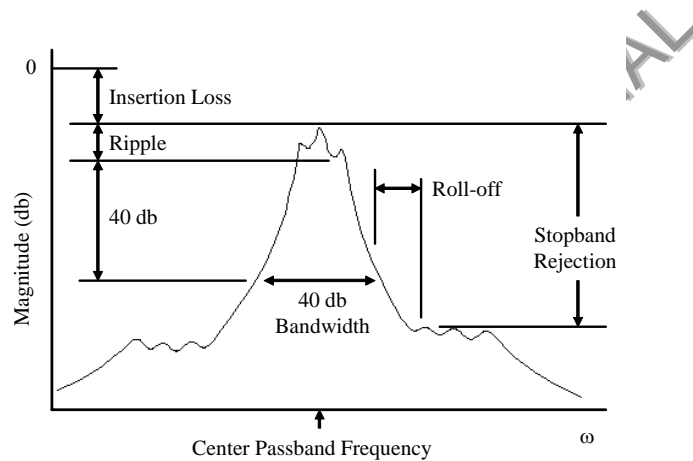


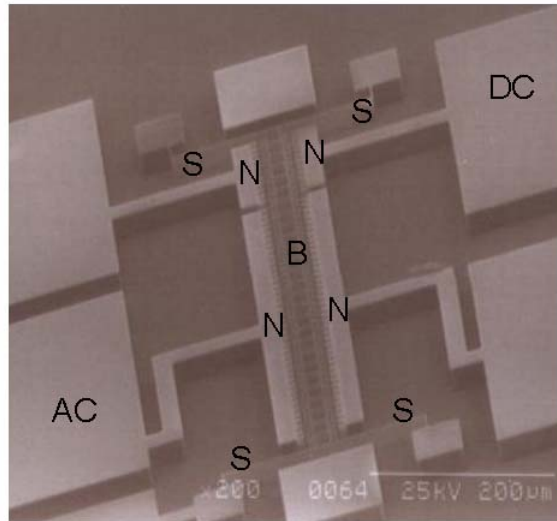
Figure 1. Transmission characteristics of a bandpass filter (Adapted from [8]).

2. Bandpass Filter Basics

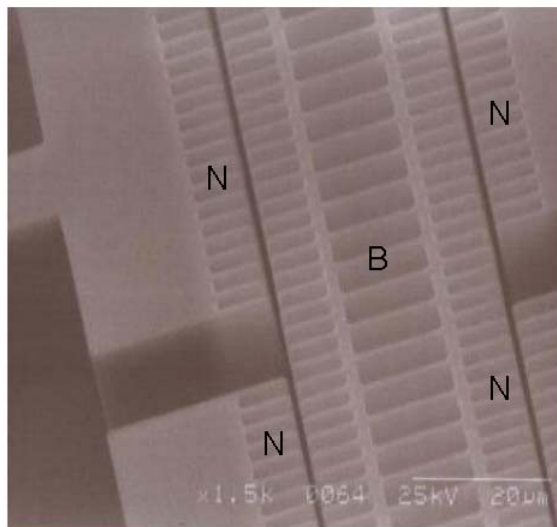
The focus in this paper is bandpass filters, which pass signals with frequency components inside a specified passband, while attenuating those outside the passband. Figure 1 highlights some of the key features considered when assessing the performance of such filters in the context of a frequency response transmission function. The following characteristics are of particular interest:

- The center passband frequency – the nominal operating frequency of the filter.
- The bandwidth – the range of frequencies that will pass through the filter with minimal loss in signal strength.
- The stopband rejection – the amount by which the signal is attenuated outside of the passband.
- The insertion loss – the reduction in signal amplitude as the signal passes through the filter.
- The sharpness of the roll-off – the width of the frequency range between the edges of the passband and the stopband.
- The flatness of the passband response – the degree to which ripples are present in the filter's passband frequency response.

An ideal filter would pass the entire signal, unaffected, in the passband, and completely reject signals outside the passband. In virtually all filter designs, this is approximated using the resonance features of a set of weakly coupled linear oscillators with very low damping, implemented using electrical circuits or mechanical oscillators, which often use surface acoustic waves (so-called SAW filters) [10-13], bulk acoustic waves (FBAR), or mechanical resonances.



(a)



(b)

Figure 2. (a) Parametrically-excited MEM oscillator. The backbone “B” is the main oscillator mass, the springs “S” provide attachment to ground as well as the mechanical restoring force, and the non-interdigitated combs “N” are used for parametric excitation. “AC” and “DC” indicate voltage sources. (b) Enlarged view of the non-interdigitated combs.

3. Employing Parametric Resonance for Filtering

As noted in the introduction, one of the distinct advantages of the MEM filters presented in this work is that they exhibit nearly ideal stopband rejection and an extremely sharp response roll-off. The basis for this is that the proposed filters are composed of parametrically-excited oscillators, rather than a chain of directly-excited oscillators. The parametric excitation is generated by applying the fluctuating voltage signal across sets of non-interdigitated comb drives, as shown in Figs. 2a and 2b, which produce a time dependent electrostatic stiffness through the resulting fringing electric fields [14]. As a result of this excitation, the oscillators remain quiescent until the frequency reaches the parametric resonance instability zone, whereupon they exhibit a rapid increase in response amplitude [9]. The resonant response amplitude is limited by nonlinearity, in contrast with the usual linear resonance, wherein damping limits the amplitude. While the presence of this phenomenon has some desirable features from a filtering point of view, the introduction of parametric instability into the system does present some problems, due to the intrinsic nature of the resulting resonant response. As described in more detail the following sections, these difficulties include:

- The bandwidth and center frequency of the passband, that is, the center and width of the unstable frequency zone depends on the amplitude of the excitation (input) signal.
- Nontrivial responses can exist outside of the passband, due to hysteresis.
- There is a nonlinear relationship between the system's input and output.
- Higher order resonances can occur.

Fortunately, most of these deficiencies can be overcome by exploiting the tunable nature of MEMS, in conjunction with some logic implementation, as presented below.

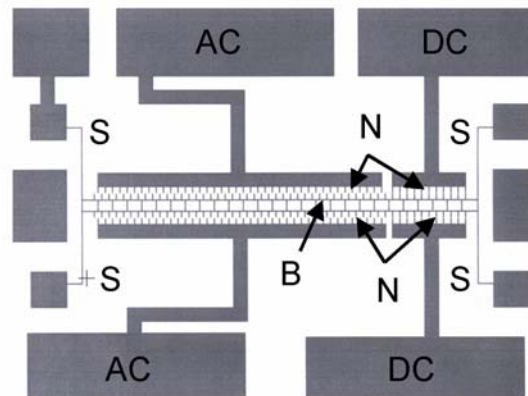


Figure 3. CAD design of a representative MEM oscillator.

4. Dynamics of a Parametrically-Excited MEMS Oscillator

To provide a basic understanding of the proposed bandpass filters, their benefits, and the difficulties that must be overcome, consider the response of a single degree of freedom MEM oscillator, such as the one shown in Fig. 2a and Fig. 3. This device, similar to those considered in [14], [15], and [4], consists of a shuttle mass, namely the oscillator's backbone "B", anchored to ground by four folded beam springs "S", and excited by an oscillating voltage applied to sets of

non-interdigitated comb drives “N”. The equation of motion for this oscillator can be expressed as [16]:

$$m\ddot{x} + c\dot{x} + F_r(x) + F_{es}(x, t) = 0, \quad (1)$$

where m represents the mass of the shuttle, c the damping coefficient (derived experimentally through logarithmic decrement methods), and $F_r(x)$ the elastic restoring force from the springs, which is accurately modeled by a cubic function of displacement,

$$F_r(x) = k_1x + k_3x^3, \quad (2)$$

which is, in general, mechanically hardening ($k_3 > 0$). The electrostatic driving and restoring forces, $F_{es}(x, t)$, are produced by two independent non-interdigitated comb drives, as shown in Fig. 2b. (The motivation for using two sets of comb drives will be described subsequently.) One set of combs utilizes a DC input voltage of amplitude V_0 and the other uses a square-rooted AC voltage signal of the form

$$V(t) = V_A \sqrt{1 + \cos(\omega t)}, \quad (3)$$

which is used to ensure isolated harmonic and parametric effects in the oscillator [9]. As with the elastic restoring force, cubic functions of displacement provide an accurate model of the resulting force, which is also proportional to the square of the respective applied voltage signals [16]. Thus, the combined force from the two sets of comb drives can be expressed as follows:

$$F_{es}(x, t) = (r_{10}x + r_{30}x^3)V_0^2 + (r_{1A}x + r_{3A}x^3)V_A^2(1 + \cos(\omega t)). \quad (4)$$

The net result is an equation of motion for the motion of the shuttle mass, which has the form:

$$m\ddot{x} + c\dot{x} + k_1x + k_3x^3 + (r_{10}x + r_{30}x^3)V_0^2 + (r_{1A}x + r_{3A}x^3)V_A^2(1 + \cos(\omega t)) = 0. \quad (5)$$

Rescaling time according to

$$\tau = \omega_0 t, \quad (6)$$

where ω_0 is the purely elastic (that is, without electrostatic effects) natural frequency,

$$\omega_0 = \sqrt{\frac{k_1}{m}}, \quad (7)$$

and rescaling the displacement according to

$$\varepsilon^{1/2} z = \frac{x}{x_0}, \quad (8)$$

where x_0 is a characteristic system length (e.g. the length of the oscillator’s backbone) and ε is a scaling parameter, results in a nondimensional equation of motion for the oscillator of the form

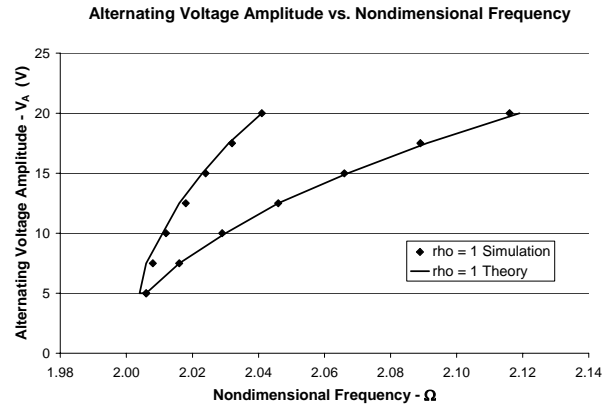
$$z'' + 2\varepsilon\zeta z' + z(1 + \varepsilon\nu_1 + \varepsilon\lambda_1 \cos(\Omega\tau)) + \varepsilon z^3(\chi + \nu_3 + \lambda_3 \cos(\Omega\tau)) = 0, \quad (9)$$

where the derivative operator and the nondimensional parameters are defined as in Table 1 [4]. Note that we have assumed small damping, which is valid for typical MEM resonators, and small excitation, which is also valid when operating near a resonance. Using this nondimensional equation of motion as a basis of study, the system response characteristics can be examined with regard to varying physical parameters and system inputs. It is important to note that many of these parameters can be selected by design of the oscillator system and the comb structures, and the forces acting on the system through the comb drives allow the system to be tuned “on the fly.” The parameter values employed in this work are taken from a preliminary design and can be found in Appendix A.

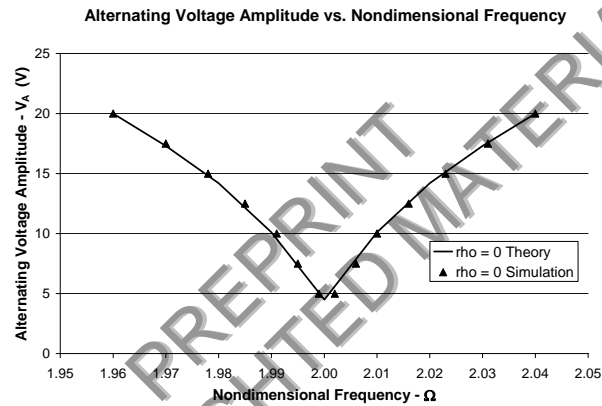
Note that this equation is not the typical nonlinear forced Mathieu equation, due to the presence of the parametric excitation acting on the cubic term, which has a significant effect on the oscillator’s response, as discussed in Section 6. The linear stability of the system is unaffected by these nonlinear effects, however, and the averaged equations (derived in Section 6) allow one to analytically approximate the instability zone for the trivial response. This is shown in Figs. 4a and 4b in terms of the $V_A - \Omega$ parameter space, that is, the physical excitation amplitude (the fluctuating voltage amplitude) versus the normalized excitation frequency. Note that the accuracy of the analytical predictions has been verified by results from simulations of the full equation of motion, from which the stability boundary is determined by examining the behavior (growth or decay) of small perturbations from the trivial response. Some important features of this stability diagram are considered next.

Definition	Nondimensional parameter
$(\bullet)' = \frac{d(\bullet)}{d\tau}$	Scaled Time Derivative
$\varepsilon\zeta = \frac{c}{2m\omega_0}$	Scaled Damping Ratio
$\varepsilon\nu_1 = \frac{r_{10}V_0^2 + r_{1A}V_A^2}{k_1}$	Linear Electrostatic Stiffness Coefficient
$\varepsilon\lambda_1 = \frac{r_{1A}V_A^2}{k_1}$	Linear Electrostatic Excitation Amplitude
$\Omega = \frac{\omega}{\omega_0}$	Nondimensional Excitation Frequency
$\chi = \frac{k_3x_0^2}{k_1}$	Nonlinear Mechanical Stiffness Coefficient
$\nu_3 = \frac{x_0^2(r_{30}V_0^2 + r_{3A}V_A^2)}{k_1}$	Nonlinear Electrostatic Stiffness Coefficient
$\lambda_3 = \frac{x_0^2r_{3A}V_A^2}{k_1}$	Nonlinear Electrostatic Excitation Amplitude

Table 1. Nondimensional parameter definitions.



(a)



(b)

Figure 4. The regions of parametric instability in the $V_A - \Omega$ parameter space. (a) The case of pure AC voltage excitation. (b) A nominal case produced through linear tuning, as described in Section 5, which results in a symmetric wedge of instability.

Due to the nature of the filtering approach described in this work, the instability zones depicted in Fig. 4 are of particular interest. First, note that the boundaries of these zones are curved, which is due to the fact that the excitation amplitude is proportional to the square of the AC voltage amplitude. A number of other observations are now described, which follow from well-known results for systems exhibiting parametric resonance [17]. Inside the “wedge of instability” the trivial response is unstable, which results in a non-zero response that is dictated by the nonlinearities present in the system. Outside of the boundary the trivial response is stable. However, this does not ensure a zero response outside the wedge, since the system can have multiple possible stable steady states, and non-trivial stable responses can occur outside the instability zone. This leads to potential hysteresis in the response, which is highly undesirable in a filter. Another characteristic of this instability is that the base of the instability wedge

originates at the nondimensional frequency of 2, and therefore filtering takes place at twice the natural frequency of the oscillator, that is, twice that of filters that utilize direct excitation. Also, the height of this base depends in a very sensitive manner on the system damping, which arises primarily from aerodynamic and structural dissipation effects in the oscillator. This implies that there is a critical AC voltage input required for the oscillator to work properly. This, however, is of minimal concern since the oscillators typically act in an environment with extremely low damping (near vacuum for testing) where quality (Q) factors can range into the thousands. Also, the input (excitation) signal can be amplified, if needed, to attain the critical excitation amplitude. Finally, the amplitude-dependent nature of the stability boundary should be noted. A direct result of this is that the system's bandwidth and center frequency depend on the excitation amplitude, some of the primary drawbacks mentioned above. These undesirable response features are overcome by the linear and nonlinear tuning schemes described in the next two sections, combined with the logic implementation presented in Section 7.

5. Manipulation of the Amplitude Dependence of the Stability Boundary

Figure 4 shows that the oscillator's activation frequency (where the trivial solution undergoes a stability change) is dependent on V_A , the amplitude of the AC voltage input. As such, when an untuned oscillator is employed as a filter, its bandwidth will be dependent on the excitation amplitude. However, it is possible to partially negate this effect through the implementation of a specific tuning scheme, namely, one in which the natural frequency of the oscillator, ω_n , is made to be dependent on V_A through a tuning of the linear electrostatic stiffness coefficient. This is accomplished by selecting the DC voltage in one set of combs to be dependent on V_A , which is the amplitude of the AC voltage that acts on the other set of combs. A description of the tuning scheme and its attendant consequences are presented here. The theoretical predictions described here are based on the averaged equations, which are presented in the following section.

To begin, we note that the signal to be filtered is the AC signal, and that the DC signal has been introduced solely for this tuning task. The DC voltage is to be dictated by the amplitude of the AC signal, as follows. A designer-specified constant of proportionality α is introduced that relates the amplitudes of the DC and AC voltage amplitudes according to

$$V_0 = \alpha V_A, \quad (10)$$

which results in the redefined parameters given in Table 2. Substituting these parameters into Eq. 9 results in a revised equation of motion, given by,

$$z'' + z = -\varepsilon(2\zeta z' + z\lambda_1(\rho + \cos(\Omega\tau)) + z^3(\chi + \nu_3 + \lambda_3 \cos(\Omega\tau))), \quad (11)$$

wherein a new tuning parameter, ρ , is introduced that relates the linear electrostatic stiffness coefficient to the linear excitation amplitude, according to

$$\rho = \frac{\nu_1}{\lambda_1} = 1 + \frac{r_{10}\alpha^2}{r_{1A}}. \quad (12)$$

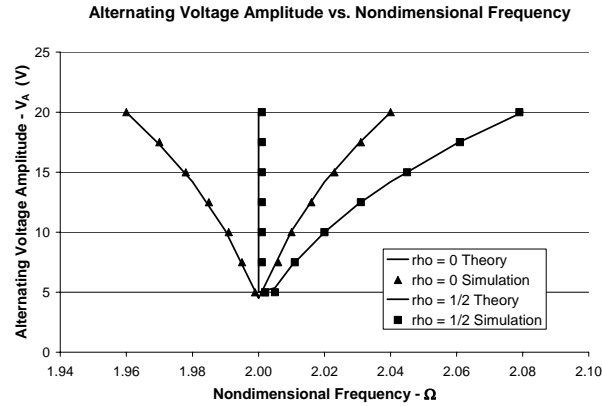
The parameter ρ represents the net effect that the AC amplitude, expressed in terms of λ_1 , has on the natural frequency of the oscillator. Specifically,

$$\omega_n = \sqrt{1 + \varepsilon\rho\lambda_1} = \sqrt{1 + \varepsilon\nu_1}. \quad (13)$$

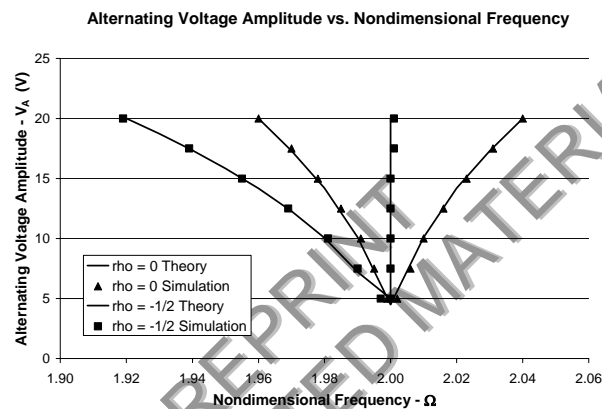
The instability zone can thus be distorted by the variation of ρ , since this produces a change in the linear natural frequency in a manner that is dependent on the input amplitude, V_A , through λ_1 . This results in rotation of the wedge of instability, away from the nominal case shown in Fig. 4b, as shown in Figs. 5a and 5b. In particular, by selecting $\rho > 0$ the wedge will rotate clockwise, and by selecting $\rho < 0$ the wedge will rotate counterclockwise. Note that one has the ability to set ρ by designing combs with the desired linear electrostatic characteristics and then selecting α accordingly. Using perturbation calculations (outlined in Section 6), it can be shown that when $r_{1A} > 0$, by selecting $\rho = 1/2$ the left stability boundary of the wedge becomes essentially vertical, as shown in Fig. 5a, and, similarly, by selecting $\rho = -1/2$ the right stability boundary becomes nearly vertical, as shown in Fig. 5b [4]. Higher order perturbation approximations can be used to improve this verticality, however, the resulting improvement in performance is minimal, so nominal values of $\rho = \pm 1/2$ are used in this work. Note that the opposite trends of those described here, in terms of the direction of the wedge rotations, occur when $r_{1A} < 0$.

Definition	Nondimensional parameter
$\varepsilon v_1 = \left(\frac{r_{10}\alpha^2 + r_{1A}}{k_1} \right) V_A^2$	Linear Electrostatic Stiffness Coefficient
$v_3 = \left[\frac{x_0^2 (r_{30}\alpha^2 + r_{3A})}{k_1} \right] V_A^2$	Nonlinear Electrostatic Stiffness Coefficient

Table 2. Redefined nondimensional parameters [4].



(a)



(b)

Figure 5. Regions of parametric instability in the $V_A - \Omega$ parameter space; for (a) $\rho = 0$ and $\rho = 1/2$ (for $r_{IA} > 0$) and (b) $\rho = 0$ and $\rho = -1/2$ (for $r_{IA} > 0$).

The aforementioned verticality, achieved by selecting $\rho = \pm 1/2$, has the distinct advantage that it renders one of the oscillator's activation frequencies to be amplitude independent and, as such, makes it act essentially like a high or low pass switch. In particular, for $r_{IA} > 0$, by selecting $\rho = 1/2$, the oscillator will act as a high pass switch, and by selecting $\rho = -1/2$ a low pass switch is achieved.

While this tuning provides a solution to one difficulty, others remain. We now turn to the possibility of non-trivial responses occurring outside of the instability zone, due to nonlinear hysteretic effects.

6. Nonlinear Tuning and Response Conditioning

As mentioned, one deficiency of the tuned oscillators presented above is that they have the propensity to feature non-zero response amplitudes outside of the wedge of instability, due to the presence of nonlinearities in the system. However, the flexibility of the comb drives in these MEM devices allows one to adjust the system nonlinearities through electrostatic forces.

Specifically, as described in [14] and [16], the cubic nonlinearity produced by electrostatic effects in the comb drives can be tuned such that the overall nonlinearity exhibits hardening, softening, or mixed hardening/softening characteristics. This is verified by considering the effective nonlinearity of the MEM oscillator, as determined through a perturbation analysis, as follows.

Equation 11 is converted to the correct form for the application of averaging by employing the standard transformation to amplitude and phase coordinates, specifically,

$$z(\tau) = a(\tau) \cos\left(\frac{\Omega\tau}{2} + \psi(\tau)\right) \quad (14)$$

$$z'(\tau) = -a(\tau) \frac{\Omega}{2} \sin\left(\frac{\Omega\tau}{2} + \psi(\tau)\right) \quad (15)$$

In order to capture the response near the parametric resonance, an excitation frequency detuning parameter σ is introduced, defined by,

$$\Omega = 2 + \varepsilon\sigma. \quad (16)$$

Equation 11 is transformed to the amplitude/phase coordinates, $a(\tau)$ and $\psi(\tau)$, and the resulting equations governing the dynamics of these variables are averaged over $4\pi / \Omega$ in the τ domain [4]. This results in the averaged equations, which are given by,

$$a' = \frac{1}{8} \varepsilon \left[-8\zeta + (2\lambda_1 + a^2\lambda_3) \sin(2\psi) \right] + O(\varepsilon^2) \quad (17)$$

$$\psi' = \frac{1}{8} \varepsilon \left[3a^2(\chi + \nu_3) + 4\lambda_1\rho - 4\sigma + 2(\lambda_1 + a^2\lambda_3) \cos(2\psi) \right] + O(\varepsilon^2). \quad (18)$$

Note that the presence of the nonlinear electrostatic parametric excitation (λ_3) leads to a complicating term in the averaged equations (as compared to the usual nonlinear Mathieu equation). Consequently, the non-trivial steady state solutions of the system take on a quite complicated form, unless some approximations are used.

Since the characteristic form of the nonlinearity (e.g., hardening, softening, etc.) is the critical feature of the response for current purposes, one can assume zero damping in order to simplify the analysis. If one examines the steady state responses in this case, it is found that the response has non-trivial branches with amplitudes given by,

$$\bar{a}_{1,2} = \sqrt{\frac{4\sigma - 2\lambda_1(2\rho - 1)}{3(\chi + \nu_3) - 2\lambda_3}}, \sqrt{\frac{4\sigma - 2\lambda_1(2\rho + 1)}{3(\chi + \nu_3) + 2\lambda_3}}, \quad (19)$$

and in certain cases additional nontrivial branches exist with amplitudes given by,

$$\bar{a}_3 = \sqrt{\frac{-2\lambda_1}{\lambda_3}}, \quad (20)$$

the latter of which appear only in parameter ranges outside of those considered here (a forthcoming paper describes these solutions in detail [18]). The signs of the terms under the square root sign determine the frequency ranges over which these branches are real, and therefore physically meaningful. In fact, it is easily seen that by selecting $\rho = \pm 1/2$ one can render the frequency (that is, the σ values) where each branch appears to be independent of the input amplitude λ_j . It is also interesting to note the role played by the nonlinearities, which differ on the two branches. To describe these effects, effective nonlinear coefficients γ_1 and γ_2 are introduced, which dictate the hardening or softening behavior of the branches, as follows,

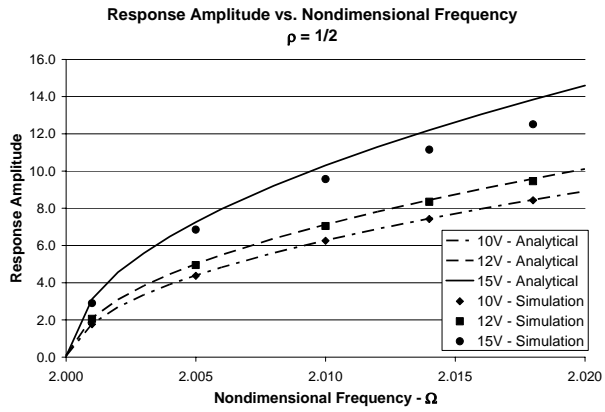
$$\gamma_1 = 3(\chi + \nu_3) - 2\lambda_3, \quad \gamma_2 = 3(\chi + \nu_3) + 2\lambda_3. \quad (21, 22)$$

Tuning the oscillator's electrostatic coefficients such that both γ_1 and γ_2 are less than zero results in an oscillator with the usual softening characteristics. Likewise, tuning the coefficients such that both γ_1 and γ_2 are greater than zero, results in an oscillator with typical hardening characteristics. Clearly mixed softening/hardening characteristics are possible as well, the details of which are left for future investigations. Note, however, that since the nonlinear coefficients are related to the input voltages (see Table 1 for χ and λ_3 , and Table 2 for ν_3), the nonlinear character of the responses may change as the input amplitude varies. This must be accounted for in the designs, and may limit the range of allowable AC input voltages for the resulting filter [18].

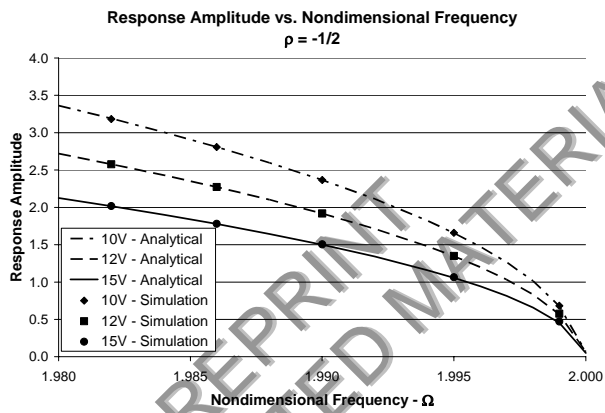
The flexibility in selecting the nature of the nonlinearity is very useful for limiting the existence of non-zero solutions outside of, or at least on one side of, the instability zone. In particular, by specifying a hardening nonlinearity for a high pass switch ($\rho = 1/2$, for $r_{1A} > 0$), non-trivial responses below the activation frequency can be avoided. Similarly, by specifying a softening nonlinearity for a low pass switch ($\rho = -1/2$, for $r_{1A} > 0$), non-trivial responses above the activation frequency can be avoided.

This nonlinear tuning can be achieved through careful design of the comb drives. As alluded to earlier, precise values of the effective nonlinear coefficients are not required, since one simply needs to maintain a particular sign of the effective nonlinearities, so that hardening or softening persists, even in the face of the mechanical (hardening) nonlinearity and the AC input. Here r_{30} and r_{3A} , two parameters determined by the geometry of the fingers of the comb drives, must be selected such that the desired response characteristics are achieved. If this cannot be achieved in conjunction with the linear tuning constraints on r_{10} and r_{1A} , it would be possible to add an additional comb drive to the oscillator, whose sole purpose is to tune the nonlinearity. It should also be noted that since the mechanical nonlinearity is hardening, one will need significant electrostatic softening in the low pass switch in order to achieve overall softening over a reasonable range of voltages.

Approximate response curves can be numerically produced from the averaged equations for general sets of parameters (including damping). Figure 6 highlights sets of curves for both a $\rho = 1/2$ oscillator with a hardening nonlinearity and a $\rho = -1/2$ oscillator with a softening nonlinearity. As predicted, each response curve originates at the chosen activation frequency ($\Omega = 2$) regardless of the AC excitation amplitude, V_A . This confirms that the instability wedges have been rotated as desired (see Fig. 5). In addition, the response quickly increases from zero to a finite amplitude immediately after activation. To confirm the validity of the perturbation calculations, results from numerical simulation of the full nonlinear equation of motion have also been included in Figs. 5 and 6. Note that the averaged solutions provide excellent accuracy at low AC voltage amplitudes, and are reasonable at larger excitation voltages.



(a)



(b)

Figure 6. Sample response curves – amplitude vs. frequency: (a) $\rho = 1/2$ and (b) $\rho = -1/2$.

7. Creating a Bandpass Filter

While the tuning schemes presented above do an excellent job of conditioning the response of an individual oscillator, they result in frequency-dependent switches, not a bandpass filter. Also, note that the switch is good at one frequency, but the other instability boundary is still amplitude-dependent, and the response will exhibit hysteresis. However, two such oscillators, tuned to act as amplitude independent switches at nearby frequency thresholds, have great potential for such use. In particular, it is possible to create a highly effective bandpass filter through the implementation scheme shown in Fig. 6.

The idea is to generate a bandpass filter which features a center passband frequency of Ω_0 and a bandwidth of $\Delta\Omega_0$, where Δ is defined to be a small parameter which describes the bandwidth as a percentage of the center frequency (see Fig. 1). This parameter may also be used to define an “effective quality (Q) factor”, where Q_{eff} is independent of system damping, as follows,

$$Q_{eff} = \frac{1}{\Delta}. \quad (23)$$

To achieve this design, two oscillators are required. One is a high pass switch (with $\rho = 1/2$ for $r_{1A} > 0$) that has been nonlinearly tuned such that it exhibits a hardening nonlinearity, which will henceforth be designated as ‘H’. The other is a low pass switch (with $\rho = -1/2$ for $r_{1A} > 0$) that has been nonlinearly tuned such that it exhibits a softening nonlinearity, which will henceforth be designated as ‘L’. In addition, both the L and H oscillators must have their linear mechanical frequencies tuned such that the base points of their respective wedges of instability are slightly shifted from Ω_0 , so that a passband is created. This can be achieved by designing the oscillators so that their zero-voltage (i.e., purely mechanical) linear instability threshold frequencies are as follows: for the L oscillator the threshold is selected to be $\Delta\Omega_0/2$ above Ω_0 , and for the H oscillator the threshold is selected to be $\Delta\Omega_0/2$ below Ω_0 . With these, the oscillators tuning is complete. A summary of the required tuning conditions for the two oscillators is given in Table 3.

Oscillator	Tuning	Condition
H Oscillator ($r_{1A} > 0$)	Zero-Voltage Linear Frequency	$\omega_{0,H} = \sqrt{\frac{k_{1,H}}{m_H}} = \frac{\Omega_0}{2} \left(1 - \frac{\Delta}{2}\right)$
	Amplitude Dependent Linear Tuning ($\rho = 1/2$)	$\left(\frac{r_{10}\alpha^2}{r_{1A}}\right)_H = -\frac{1}{2}$
	Hardening Nonlinearity	$\gamma_{1H} > 0$ and $\gamma_{2H} > 0$
L Oscillator ($r_{1A} > 0$)	Zero-Voltage Linear Frequency	$\omega_{0,L} = \sqrt{\frac{k_{1,L}}{m_L}} = \frac{\Omega_0}{2} \left(1 + \frac{\Delta}{2}\right)$
	Amplitude Dependent Linear Tuning ($\rho = -1/2$)	$\left(\frac{r_{10}\alpha^2}{r_{1A}}\right)_L = -\frac{3}{2}$
	Softening Nonlinearity	$\gamma_{1L} < 0$ and $\gamma_{2L} < 0$

Table 3. Summary of tuning requirements for bandpass filtering.

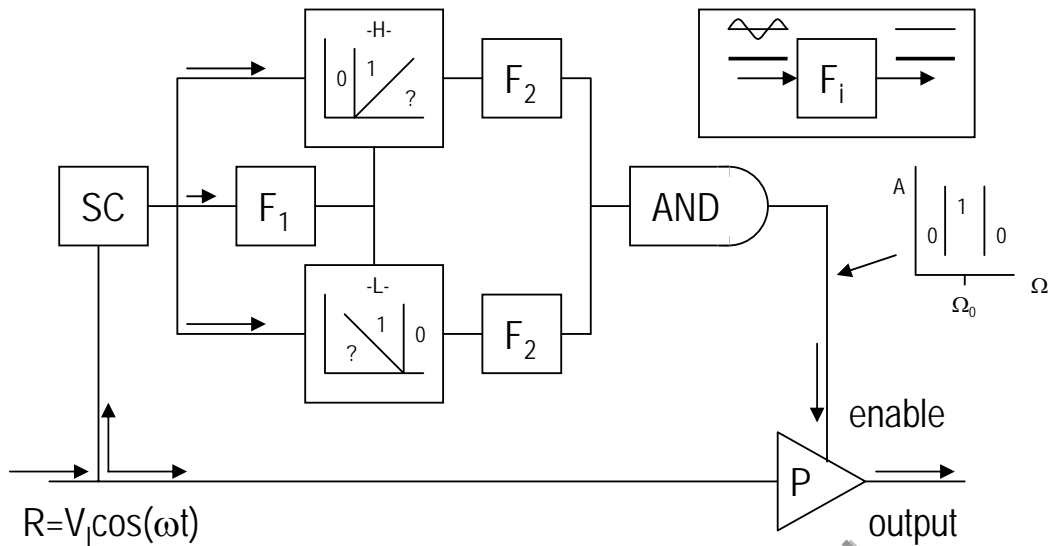


Figure 7. Hardware implementation scheme (From [4]).

Once the two oscillators have been tuned in accordance with the conditions set forth in Table 3, they are ready for implementation in the filter system presented in Fig. 7. This system is designed to function as follows. A harmonic input signal, R , of the form $R = V_I \cos(\omega t)$ is supplied to the system. This signal travels to a signal conditioner (SC) that produces an excitation signal appropriate for the oscillators' comb drives, namely the square-rooted input described in Section 4. This signal is then used to drive both the H and L oscillators, and is also provided to the block designated F_1 . This block represents an AC to DC converter that produces the amplitude of R , namely V_I (which is monotonically related to V_A), or some proportion thereof. This DC signal is sent to the oscillators, where it is used to drive the two resonators, and to tune each oscillator through their linear tuning parameters, $\rho = \pm 1/2$ (recall that the ρ tuning is set by α , which sets V_0 in relation to V_A). Each oscillator, acting as described in previous sections, filters the provided input signal and acts as a switch, producing a zero (in practice, the noise floor) or oscillatory response, depending on the frequency of the excitation signal. The respective signal from each oscillator is then sent to another block designated F_2 which converts the signal into a constant voltage, or to a digital signal. For example, the block may produce a 0 when the oscillator's output is zero (noise floor) and 1 when the output is oscillating. The signal from each F_2 block then proceeds to an AND junction, which provides a non-zero signal to the enabling block P only when the frequency of the input signal falls within the desired bandwidth. If the enabling device P receives a non-zero signal, it allows the original filter input to pass unimpeded, otherwise, it blocks the signal. The result is a bandpass filter with ideal stopband rejection and optimal roll-off in its frequency response.

To verify the operation of the filtering scheme presented in Fig. 7, numerical simulations of the system were carried out using Simulink™. As Fig. 8 shows, the results for a bandpass filter designed with an effective quality factor of 500 are essentially as expected. The filter bandwidth is nearly amplitude independent (note the horizontal scale), and could be made even more so by improving the tuning parameter, ρ . In addition, the attenuation outside of the passband is absolute, which verifies that the filter's stopband rejection is ideal.

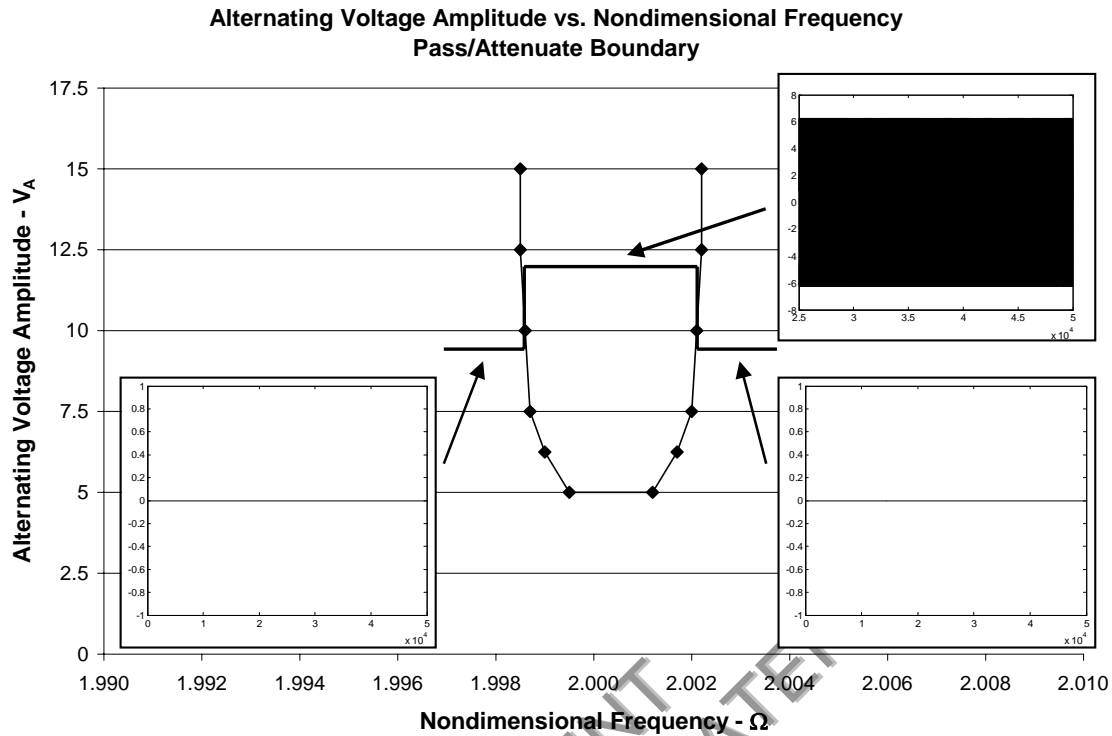


Figure 8. Simulation results from the filter system of Fig. 7. Data points are frequency thresholds for the passband boundaries at various AC amplitude levels. The insets show the system outputs at the points indicated.

8. Conclusions

Filtering based on parametric excitation has some very attractive features, as summarized in Fig. 8. For the implementation considered here, the only obvious drawback of note is that a damping-dependent critical AC excitation amplitude is required for operation (which can be addressed by restricting the input voltage to a specified range). Other potential concerns for implementation of such a filter include: the fact that the insertion loss of the physical system cannot yet be quantified, since this will depend on the hardware implemented for the filter; higher order resonances may appear in the system, which will lead to non-trivial responses well away from the passband; and design robustness issues may arise, for example, the required accuracies of the linear tuning strategy that rotates the wedge, temperature sensitivity, etc.. Also of interest are the transient behavior and the phase response of the parametrically-excited oscillators in question. In particular, the settling time required for an oscillator to reach steady state and the steady-state phase characteristics need further investigation. Preliminary simulation results indicate that the oscillators described here exhibit settling times comparable to those of linear oscillators with the same level of damping. However, due to the frequency dependence of the settling time in parametrically-excited systems, this result is valid only in a frequency domain near the passband center frequency, since the system's time constant approaches infinity at the stability boundaries, where bifurcations occur. The phase behavior of the filter can be easily quantified from the averaged equations. These issues are currently being addressed in ongoing investigations, which include experimentation.

While this paper focused on bandpass filters, it is worth noting that an equally ideal band gap filter can be produced by simply changing block P such that it enables with a zero amplitude signal instead of a non-zero amplitude signal. It is also expected that these parametric-based frequency switches can be used to develop high and low pass filters. The ultimate goal of this line of work is to achieve fully functional filters wherein the parametrically-excited MEM oscillators and the associated circuitry are integrated into a single chip.

9. Acknowledgements

This work is supported by the AFOSR under contract F49620-02-1-0069. SWS would like to thank the Mechanical Engineering Department at the University of California, Santa Barbara (UCSB) for their hospitality during a sabbatical visit, during which the work for this paper was completed. In addition, the authors are grateful to Professor Jeff Moehlis and Barry Demartini of UCSB for useful input on the analysis of the oscillator equation and the preliminary designs of the MEMS oscillators, respectively.

10. Appendix A: Design Parameters

$\rho = 1/2$ Oscillator	$\rho = -1/2$ Oscillator
$k_1 = 10 \mu\text{N}/\mu\text{m}$ (0.69 lbf/ft)	$k_1 = 10 \mu\text{N}/\mu\text{m}$ (0.69 lbf/ft)
$k_3 = 0.05 \mu\text{N}/\mu\text{m}^3$ (3.2E8 lbf/ft ³)	$k_3 = 0.05 \mu\text{N}/\mu\text{m}^3$ (3.2E8 lbf/ft ³)
$x_0 = 1.0 \mu\text{m}$ (3.2E-6 ft)	$x_0 = 1.0 \mu\text{m}$ (3.2E-6 ft)
$m = 4.0528\text{E-}10$ kg (8.9349E-10 lbm)	$m = 4.0528\text{E-}10$ kg (8.9349E-10 lbm)
$\xi = 0.01$	$\xi = 0.01$
$r_{1A} = 2.00\text{E-}3 \mu\text{N}/\mu\text{mV}^2$ (1.37E-4 lbf/ftV ²)	$r_{1A} = 2.00\text{E-}3 \mu\text{N}/\mu\text{mV}^2$ (1.37E-4 lbf/ftV ²)
$r_{10} = -5.00\text{E-}4 \mu\text{N}/\mu\text{mV}^2$ (-3.43E-5 lbf/ftV ²)	$r_{10} = -5.00\text{E-}4 \mu\text{N}/\mu\text{mV}^2$ (-3.43E-5 lbf/ftV ²)
$r_{3A} = 1.00\text{E-}3 \mu\text{N}/\mu\text{m}^3\text{V}^2$ (6.37E6 lbf/ft ³ V ²)	$r_{3A} = 1.00\text{E-}3 \mu\text{N}/\mu\text{m}^3\text{V}^2$ (6.37E6 lbf/ft ³ V ²)
$r_{30} = -2.50\text{E-}4 \mu\text{N}/\mu\text{m}^3\text{V}^2$ (-1.59E6 lbf/ft ³ V ²)	$r_{30} = -7.50\text{E-}4 \mu\text{N}/\mu\text{m}^3\text{V}^2$ (-1.59E6 lbf/ft ³ V ²)

11. References

- [1] Taylor, J. T., and Huang, Q., eds., 1997, *CRC Handbook of Electrical Filters*, CRC Press, Boca Raton, Florida, pp. 45-142, 353-418.
- [2] Johnson, R. A., Borner, M., and Konno, M., 1971, "Mechanical Filters - A Review of Progress," *IEEE Transactions of Sonics and Ultrasonics*, **SU-18**(3), pp. 155-170.
- [3] Nguyen, C. T.-C., 1999, "Micromechanical Filters for Miniaturized Low-Power Communications," 3673-19, *Proceedings of SPIE: Smart Structures and Materials 1999: Smart Electronics and MEMS*, V. K. Varadan, ed., **3673**, pp. 55-66.
- [4] Shaw, S. W., Turner, K. L., Rhoads, J. F., and Baskaran R., 2004, "Parametrically Excited MEMS-Based Filters," *Proceedings of the IUTAM Symposium on Chaotic Dynamics and Control of Systems and Processes in Mechanics*, (to be published).
- [5] Piekarski, B., DeVoe, D., Dubey, M., Kaul, R., Conrad, J., Zeto, R., 2001, "Surface Micromachined Piezoelectric Resonant Beam Filters," *Sensors and Actuators A: Physical*, **91**(3), pp. 313-320.
- [6] Lin, L., Howe, R. T., and Pisano, A. P., 1998, "Microelectromechanical Filters for Signal Processing," *Journal of Microelectromechanical Systems*, **7**(3), pp. 286-294.
- [7] Nguyen, C. T.-C., 1995, "Micromechanical Resonators for Oscillators and Filters," *Proceedings, 1995 IEEE International Ultrasonics Symposium*, pp. 489-499.
- [8] Wang, K. and Nguyen, C. T.-C., 1997, "High-Order Micromechanical Electronic Filters," *Proceedings, 1997 IEEE International Micro Electro Mechanical Workshop*, pp. 25-30.
- [9] Turner, K. L., Miller, S. A., Hartwell, P. G., MacDonald, N. C., Strogatz, S. H., and Adams, S. G., 1998, "Five Parametric Resonances in a Microelectromechanical System," *Nature*, **396**, pp. 149-152.
- [10] Machui, J., Bauregger, J., Riha, G., and Schropp, I., 1995, "SAW Devices in Cellular and Cordless Phones," *1995 IEEE Ultrasonics Symposium Proceedings*, pp. 121-130.
- [11] Wright, P. V., 1992, "A Review of SAW Resonator Filter Technology," *1992 IEEE Ultrasonics Symposium Proceedings*, pp. 29-38.
- [12] Ishihara, F., Koyamada, Y., and Yoshikawa, S., 1975, "Narrow Band Filters Using Surface Acoustic Wave Resonators," *1975 IEEE Ultrasonics Symposium Proceedings*, pp. 381-383.
- [13] Tiersten, H. F., and Smythe, R. C., 1975, "Guided Acoustic Surface Wave Filters," *1975 IEEE Ultrasonics Symposium Proceedings*, pp. 293-294.
- [14] Adams, S. G., Bertsch, F., and MacDonald, N. C., 1998, "Independent Tuning of Linear and Nonlinear Stiffness Coefficients," *Journal of Microelectromechanical Systems*, **7**(2), pp. 172-180.
- [15] Zhang, W., Baskaran, R., and Turner, K. L., 2003, "Tuning the Dynamic Behavior of Parametric Resonance in a Micromechanical Oscillator," *Applied Physics Letters*, **82**(1), pp. 130-132.

[16] Zhang, W., Baskaran, R., and Turner, K. L., 2002, "Effect of Cubic Nonlinearity on Auto-Parametrically Amplified Resonant MEMS Mass Sensor," *Sensors and Actuators A: Physical*, **102**(1-2), pp. 139-150.

[17] Nayfeh, A. H., and Mook, D. T., 1979, *Nonlinear Oscillations*, Wiley, New York.

[18] Rhoads, J. F., Shaw, S. W., Turner, K. L., Moehlis, J., and DeMartini, B. E., 2004, "On the Response of Systems with Generalized Parametric Excitation Including Application to MEMS," (in preparation).

PREPRINT
COPYRIGHTED MATERIAL